Colloids and Surfaces A 557 (2018) 14–19

Contents lists available at ScienceDirect

Colloids and Surfaces A

journal homepage: www.elsevier.com/locate/colsurfa

PTA-based ruthenium complexes as photosensitizers for dye-sensitized solar cells

Benjamin Sierra-Martin[a,*], Ana Maldonado-Valdivia[a], Manuel Serrano-Ruiz[b], Antonio Romerosa[b], Antonio Fernandez-Barbero[a,c]

[a] NanoLab, Department of Chemistry and Physics, University of Almeria, 04120, Almeria, Spain
[b] Inorganic Chemistry Lab-CIESOL, Department of Chemistry and Physics, University of Almeria, 04120 Almeria, Spain
[c] Institute of Applied Chemical Sciences, Universidad Autonoma de Chile, Santiago, Chile

GRAPHICAL ABSTRACT

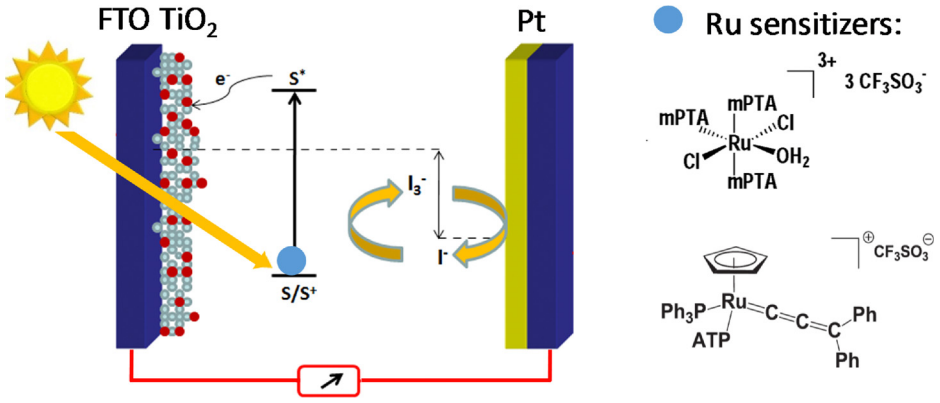

ARTICLE INFO

Keywords:
Ruthenium complex
Dye
Sensitizer
Solar cell
PTA

ABSTRACT

Two novel ruthenium complexes are synthesized, photo-characterized and tested as photosensitizers in dye-sensitized solar cells (DSCs): $[RuCl_2(mPTA)_3(H_2O)](CF_3SO_3)_3$ (**C1**) (m: methyl; PTA: 3,5,7-triaza-phosphaadamantane) and $[Ru(C=C=CPh_2)Cp(PTA)(PPh_3)](CF_3SO_3)$ (**C2**). The complexes are soluble in organic solvents and, interestingly, in water, which makes them useful for water-based photochemical processes. They possess excellent photon-absorption over a wide range of the spectrum with intense peaks at ~ 330 nm for both sensitizers. A second peak is found for **C2** at 525 nm, wider than the corresponding to the N719 standard dye. DSCs using these sensitizers are evaluated against different electrolytes. The solar cell performance was similar for both complexes and strongly dependent on the electrolyte nature, with a maximum conversion efficiency of 0.32% for the iodide/triiodide electrolyte.

1. Introduction

The use of dye-sensitized solar cells (DSCs) is a well stablished strategy for solar energy conversion because of their efficiency, inexpensive manufacturing and environmental friendly nature [1,2]. DSCs are sandwich-type electrochemical devices based on

* Corresponding author.
E-mail addresses: bsierra@ual.es (B. Sierra-Martin), amaldonado@ual.es (A. Maldonado-Valdivia), mserrano@ual.es (M. Serrano-Ruiz), romerosa@ual.es (A. Romerosa), afernand@ual.es (A. Fernandez-Barbero).

https://doi.org/10.1016/j.colsurfa.2018.06.003
Received 20 March 2018; Received in revised form 1 June 2018; Accepted 2 June 2018
Available online 04 June 2018
0927-7757/

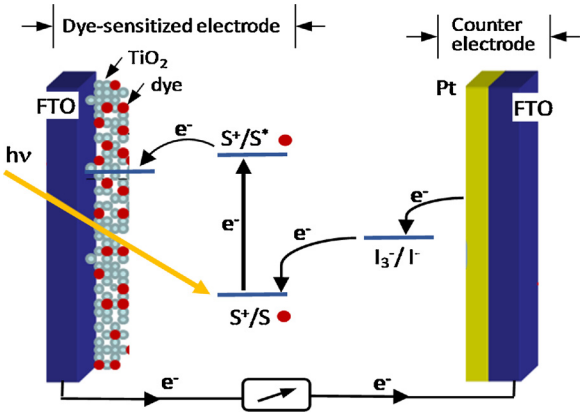

Fig. 1. Schematic representation of a dye-sensitized solar cell and the electron transfer mechanism involved in energy conversion.

nanocrystalline metal oxide semiconductors sensitized by molecular dyes [3,4]. The dye (or photosensitizer) is able to absorb over a wide range of the solar spectrum to reach its excited state, then producing electrons injected into the conduction band of the semiconductor (photoelectrode), as depicted in Fig. 1. The semiconductor often consists of a mesoporous TiO_2 film deposited on a transparent fluorine-doped tin oxide (FTO) conducting glass; this provides a large surface area to maximize the light absorption while ensures the dye-electrolyte electrical connection. Injected electrons flow towards the counter electrode, a platinized FTO glass substrate, and are transferred to the redox pair present in the electrolyte (usually I^-/I_3^-). The circuit is completed when the oxidized dye is regenerated to its ground state by electron donation from the electrolyte. As a result, DCSs perform an electrical work through a regenerative photo-electrochemical cycle without consumption of chemical species [5].

DSCs use indistinctly natural or synthetic dyes to harvest energy from light [6]. Artificial dyes, usually based on transition metal coordination complexes such as Ru, Os and Pt, are widely employed since they yield greater efficiencies [7,8]. Ruthenium-based complexes satisfy a few key requirements to work properly, such as photon absorption across a broad range of wavelengths, chelation to TiO_2 surface, and chemical stability. Among these complexes, polypyridyl ruthenium dyes such as the well-known N719, N3, N749 have been used because of their broad-spectrum absorption, excellent redox characteristics and high stability. In addition, they bound strongly to the mesoporous TiO_2 film through carboxylate or phosphonate groups, thus ensuring an efficient electron injection into the photoelectrode. So far, these dyes are considered as benchmark reference sensitizers, achieving high conversion efficiencies [9,10].

Nowadays, considerable development is focused on the design of new strategies to enhance the dye-sensitized solar cell performance [11–14]. Progress on dye optimization is usually performed through systematic variation of ligands and other substituent groups [15,16]. This strategy allows to control the photon absorption properties as well as the electronic coupling between the sensitizer excited state and the semiconductor conduction band, which in turn determine the efficiency of the solar cell. Advances on the design of ruthenium-based sensitizers and their applications to DSCs have been extensively reviewed [17–20].

In this work, two PTA-based ruthenium complexes are synthesized and tested as DSC sensitizers: $[RuCl_2(mPTA)_3(H_2O)](CF_3SO)_3$ (**C1**) and $[Ru(C=CPh_2)Cp(PTA)(PPh_3)](CF_3SO_3)$ (**C2**), with m: methyl, and PTA: 3,5,7-triaza-phosphaadamantane. PTA ligands make these complexes soluble in aqueous solvents, becoming them useful for water-based photochemical processes [21]. Both complexes present intense photon-absorption bands at ~ 330 nm and **C2** also displays a much stronger absorption at 525 nm. Moreover, chelation to the titania film can be accomplished via the PTA groups, similarly to the anchoring provided by phosphate groups [22]. The efficiency of DSCs containing the complexes in combination with three electrolytes is evaluated and compared to N719. The electrochemical behavior is similar for both complexes with a strong influence of the electrolyte nature.

2. Materials and methods

2.1. Materials

Conducting glass plates (FTO) (F-doped SnO_2, with resistance 11–13 Ω/sq, Nippon Sheet Glass) are used to fabricate the electrodes of the DSCs. TiO_2 and Pt films are fabricated from TiO_2 (P-25, Degussa), Triton X-100 (Merck) and H_2PtCl_6 (Aldrich). Iodine (99.9%, Aldrich), LiI (99.9%, Aldrich), 4-tert-butylpyridine (TPB) (96%, Aldrich), 1-methyl-3-propylimidazolium iodide (MPII) (98%, Aldrich), N-Methylbenzimidazole (NMBI) (99%, Aldrich), Guanidinium thiocyanate (GNCS) (99%, Sigma) and 3-methoxypropionitrile (98%, Aldrich) are employed to prepare the electrolyte solutions. The dye N719 (95%) and all the other chemicals are purchased from Sigma-Aldrich with reagent grade and used as received.

2.2. Synthesis and characterization of the ruthenium complexes

All reactions were carried out under dry nitrogen atmosphere by standard Schlenk-tube techniques. Solid complexes were collected on sintered glass-frits and washed as described later. The following products for the synthesis were prepared according to reported procedures: PTA [23], $[RuCl_2(PPh_3)_2]$ [24,25], [RuCpCl(PPh3)2] [26] and [RuCpCl (PTA)(PPh3)] [27,28].

2.2.1. Complex *C1*: $[RuCl_2(mPTA)_3(H_2O)](CF_3SO_3)_3$

We first prepared the compound $mPTA(CF_3SO_3)$, which is one of the reactants to accomplish the synthesis of complex **C1**. To this end, $MeCF_3SO_3$ (0.56 mL, 5.08 mmol) was added to a stirred PTA (0.6 g, 3.82 mmol) solution prepared in $CHCl_3$ (60 mL). A white suspension is formed, further stirred for 30 min at room temperature. The resulting white precipitate was filtered, washed against $CHCl_3$ and air-dried. Yield: 91.3%.

Complex **C1** was synthesized by reacting $mPTA(CF_3SO_3)$ and $[RuCl_2(PPh_3)_2]$ in MeOH according to Scheme 1. The complex $[RuCl_2(PPh_3)_2]$ (450 mg, 0.47 mmol) was dissolved in MeOH (60 mL) and then $mPTA(CF_3SO_3)$ (460 mg, 1.43 mmol) was added. The MeOH used for the synthesis was not dried, providing the water required for the reaction. After 6 h of reaction at room temperature, a yellow–orange solution was obtained. Next, the solvent was reduced to 15 mL and 20 mL of Et_2O were added. The yellow precipitate was finally filtered under inert atmosphere, washed against Et_2O and vacuum-dried. Yield: 84%.

The yellow complex **C1** is soluble and stable in water at room temperature ($S_{25\,°C}$ = 89 mg mL^{-1}). The molecular structure consists of a distorted octahedral ruthenium atom bonded to two mPTA trans to each other, two Cl ligands trans to each other and one mPTA trans to

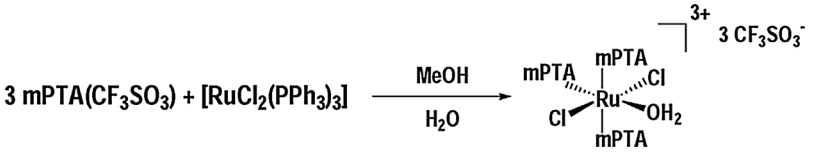

Scheme 1. Synthesis of the ruthenium complex **C1**.

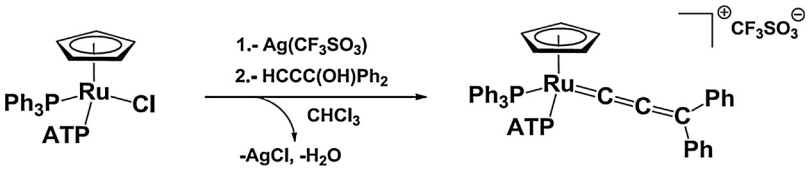

Scheme 2. Synthesis of the ruthenium complex **C2**.

one water molecule [29]. The positive charge of the complex is balanced by three CF_3SO_3 - counter-ions. Characterization data can be found in the supplementary material.

*2.2.2. Complex **C2**: [Ru(C = C=CPh$_2$)Cp(PTA)(PPh$_3$)](CF$_3$SO$_3$)*

The allenylidene-ruthenium complex was prepared as described in Scheme 2. Ag(CF3SO3) (0.03 g, 0.12 mmol) dissolved in CHCl3 (2 mL) was added to a stirred solution of [RuCpCl(PTA)(PPh3)] (0.072 g, 0.12 mmol) prepared in 30 mL of CHCl3. The solution reacted with 1,1-diphenyl-2-propyn-1-ol (0.18 g, 0.81 mmol) for 5 min at room temperature followed by 2 h reaction at refluxing temperature. The resulting mixture was filtered to remove the precipitated AgCl, yielding a purple solid after solvent evaporation. The solid corresponding to complex **C2** was washed against Et2O (2 x 5 mL) and dried under vacuum. Yield: 94%.

Complex **C2** is soluble in common organic solvents and slightly soluble in water (S25 °C = 0.1 mg mL^{-1}). The complex formation is confirmed by $^{13}C\{^1H\}$ NMR [30]. Spectra reveal a neat triplet slightly below 293.7 ppm corresponding to the allenylidene α-carbon coupled to the two phosphines P-atoms. Signals ascribable to both β- and γ-carbons are detected at the expected chemical shifts. The complex keeps its nature in solid state, as confirmed by the characteristic allenylidene stretching absorption band observed by IR spectra, $\nu_{(C=C=C)}$: 1930 cm^{-1}. The cone angles of the PPh3 and PTA phosphines are obtained from the structure of a parent complex, as **C1** does not form crystals. These angles are 133° for the PPh3 and 109° for the PTA, in agreement with those found for other ruthenium complexes with PPh3 and PTA ligands [30]. Further characterization results are shown in the supplementary data.

2.3. FTO electrical resistance

The influence of the thermal treatment on the FTO electrical resistance, R_S, was studied according to the Van der Pauw method [31]. Initial resistance value, R_S = (12.60 ± 0.20) Ω/sq, changes to Rs = (13.45 ± 0.15) Ω/sq after cleaning with isopropanol and activation by temperature (420 °C, 30 min). The FTO is a suitable material for solar cell fabrication, provided that the thermal treatment does not increase significantly the sheet resistance [32].

2.4. Fabrication of photoelectrodes

A concentrated paste of TiO_2 (15 wt.%) was prepared by dispersing TiO_2 nanoparticles in a mixture of ethanol (61 wt.%) and nitric acid (24 wt.%) under 12 h stirring at room temperature. Surfactant Triton X-100 (0.2 wt.%) was added and the mixture stirred for additional 12 h.

FTO substrates were covered with transparent adhesive tape (Scotch, 50 µm in thickness), leaving a square-shaped free surface of ~0.4 cm^2. A drop of the TiO_2 paste was spread using a glass rod over the square area by the so called doctor-blade technique. The paste was allowed to dry at room temperature for 1 h under ethanol atmosphere. The substrate was placed into a muffle furnace (450 °C, 1 h) to calcine the paste, then forming the mesoporous TiO_2 film. This procedure yields high quality TiO_2 films without granular features or cracks on the surface [33].

The different ruthenium complexes were adsorbed onto the TiO_2 film by adding an excess of dye solution. The reference dye N719 was prepared in ethanol at 3.10^{-4} M, **C1** in H_2O at 3.10^{-2} M, and **C2** in chloroform at 3.10^{-3} M. Adsorption processes were conducted in dark at room temperature for 24 h. The non-adsorbed dye was removed by rinsing with ethanol.

The platinized counter electrodes were made by coating FTO substrates with a thin layer of Pt. A droplet of the H_2PtCl_6 solution (0.01 M in ethanol) was spread on the surface before heating at 380 °C for 20 min.

2.5. DSC assembly and chraracterization

The solar cells were assembled following the procedure stablished by Ito et al. [34,35]. The dye-sensitized electrode and the counter electrode were assembled in a sandwich-type cell using a thermal adhesive film (Dupont Surlyn, 60 µm) to set the inter-electrode gap and make the solar cell airtight. The electrolytes penetrate the gap by capillary action from a tiny hole drilled on the counter electrode. As a result, we obtain solar cells with an active electrode area of 0.36 cm^2.

Photocurrent density-voltage (J–V) curves were determined under direct sun radiation. The solar irradiation, measured with a thermopile-based pyranometer, was similar in all experiments: 399.3 W/m^2 (admitting 5% error tolerance). J–V curves were determined by digital source meters without any external bias. The electrical data were averaged over three samples in each case, which also allowed to check the reproducibility.

3. Results and discussion

3.1. UV–vis properties

The UV–vis absorption spectra were recorded using a high resolution diode array spectrophotometer (HR4000, Ocean Optics). Fig. 2 plots the normalized absorption vs wavelength of the ruthenium complexes, including the well-known spectrum of N719 in ethanol. The electronic spectrum of complex **C1** in water is characterized by a strong absorption peak at 326 nm and a smaller one at 448 nm; the absorption

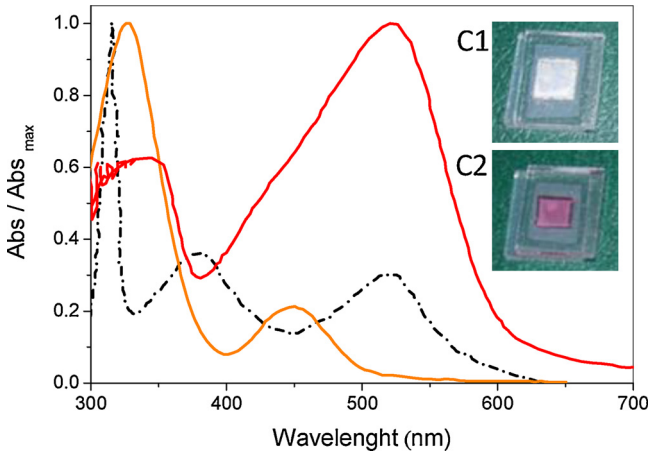

Fig. 2. UV–vis absorption spectra of the ruthenium complexes; N719 was prepared in ethanol at 3.10^{-4} M (dot line), complex **C1** in H_2O at 3.10^{-2} M (orange), and complex **C2** in chloroform at 3.10^{-3} M (red). Inset: Dye-sensitized solar cells prepared with the ruthenium complexes **C1** and **C2**. Glass substrates shift allows the electrical contacts (For interpretation of the references to colour in this figure legend, the reader is referred to the web version of this article).

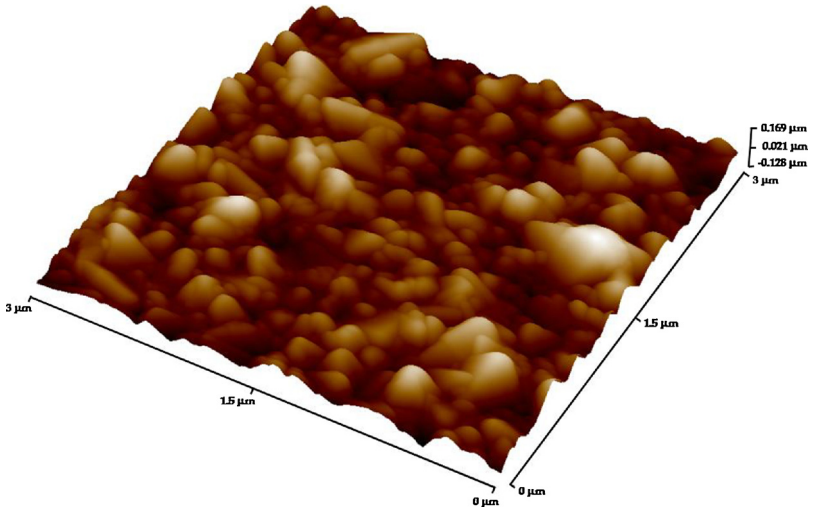

Fig. 3. AFM scan of the platinized counter electrode. The image was taken with a microscope Veeco Innova (model 840-012-711) in tapping mode by scanning an area of 3 µm × 3 µm with 1024 lines resolution at a scan rate of 0.6 µm/s.

coefficient was $\varepsilon_{max} \approx 10^3\ M^{-1}cm^{-1}$. On the other hand, complex **C2** in chloroform displays a peak at 338 nm as well as a broad absorption band in the visible range, with the maximum located at 520 nm. This band matches to one of the N719 absorption peaks, being the **C2** band wider. Furthermore, the first peak of both dyes appears at similar wavelengths than the corresponding to the maximum absorption of N719 (315 nm).

The electronic properties of the ruthenium complexes arise from ligand-centered transitions (LCCT), metal-centered or d-d transitions (MC) as well as metal-to-ligand charge transfer transitions (MLCT). The absorption peaks appearing in the UV range are due to LCCT transitions. At higher wavelengths, the absorption comes from MC and MLCT transitions [36]. The ruthenium complexes show absorption properties similar to those of N719, with strong absorption bands covering a wide range of the spectrum. In view of these results, the ruthenium complexes seem to meet the requirements to sensitize DSCs.

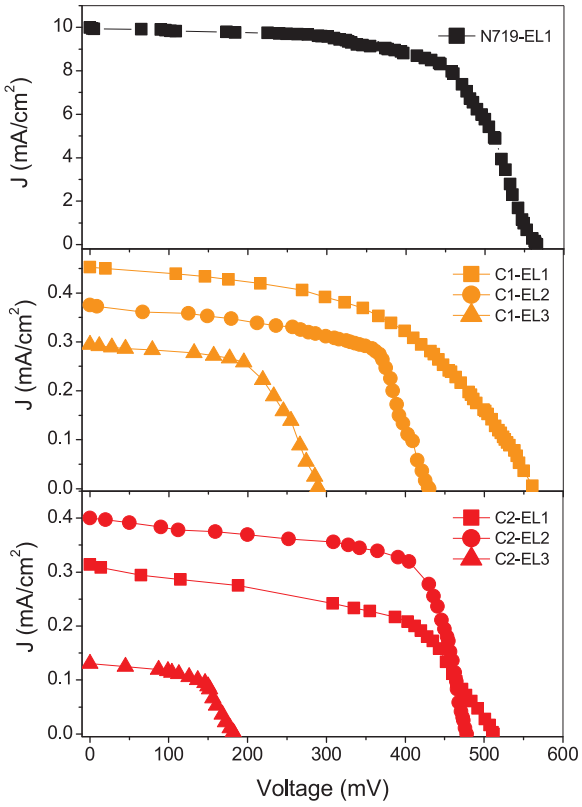

Fig. 4. J–V curves for dye-sensitized solar cells made with different dyes: a) N719; b) Complex **C1**; c) Complex **C2**. DSCs are tested using electrolytes EL1-3.

3.2. Morphology of the Pt electrode

Atomic Force Microscopy (AFM) was used to characterize the morphology, topography and roughness of the counter electrode as these parameters influence the solar cell performance. Fig. 3 shows an AFM surface image of the Pt film deposited on FTO substrate. The image shows a highly textured Pt electrode with 32.3 nm roughness. A surface area of 12.60 µm^2 was measured for 9.0 µm^2 scanning area (surface/area ratio = 1.4). This results is very similar to that obtained by Tsai and coworkers [37]. These authors found the best solar cell performance for platinized electrodes with roughness = 28.3 nm and surface/area ratio = 1.17, confirming that our deposition method optimizes the morphology of the Pt counter electrode. The resulting high roughness and surface area enhance the catalytic ability of the electrode for I_3^- ions reduction and charge exchange at the Pt/electrolyte interface. As a result, the conversion efficiency of the solar cell is expected to enhance by 10% respect to other electrode morphologies [37].

3.3. Solar cell performance

Cells will be named Cx-ELy, being x, y the numbers of the complex (C) and electrolyte (EL). Three electrolytes are used: EL1: 0.05 M I_2, 0.5 M LiI, 0.5 M 4-tert-butylpyridine (TBP) in 3-methoxypropionitrile; EL2: 0.05 M I_2, 0.5 M LiI in 3-methoxypropionitril; EL3: 1.0 M PMII, 0.5 M NMBI, 0.1 M GNCS in 3-methoxypropionitrile. Electrolytes EL1, EL2 are based on the iodide/triiodide redox couple that is considered one of the most efficient charge mediator [32]. Electrolyte EL3 is a liquid ionic composed of imidazolium salts as a source of iodide. It is widely used because of their improved chemical and thermal stability, which is a key requirement for long-lived DSCs [38]. For each complex-electrolyte combination, three solar cells were fabricated to check reproducibility.

Fig. 4 shows average current density–voltage curves for DSCs. Curves allow accessing the electrical parameters: open circuit voltage, V_{OC}; short circuit current density, J_{SC}; fill factor, FF; and overall efficiency, η. The last one represents the percentage amount of solar light converted to electrical output. These parameters are averages from three measurements and are summarized in Table 1. A reference cell is made with dye N719 and electrolyte EL1 (N719-EL1) for comparison. It

Table 1
Electrical parameters of the DSCs fabricated with the ruthenium complexes **C1**, **C2** in combination with different electrolytes (EL1-EL3). N719-EL1 stands for the reference cell.

Solar cell	VOC (mV)	JSC (mA/cm2)	FF	Efficiency, η (%)
N719-EL1	568 ± 1	9.77 ± 0.05	0.63 ± 0.03	8.8 ± 0.5
C1-EL1	550 ± 1	0.444 ± 0.008	0.529 ± 0.011	0.324 ± 0.011
C1-EL2	396 ± 1	0.378 ± 0.008	0.623 ± 0.013	0.233 ± 0.024
C1-EL3	256 ± 1	0.275 ± 0.008	0.575 ± 0.015	0.101 ± 0.024
C2-EL1	510 ± 1	0.306 ± 0.008	0.528 ± 0.006	0.206 ± 0.003
C2-EL2	492 ± 1	0.397 ± 0.008	0.662 ± 0.015	0.324 ± 0.003
C2-EL3	180 ± 1	0.122 ± 0.008	0.50 ± 0.04	0.028 ± 0.004

yields an efficiency of 8.8%, as expected according to previous works [35,39]; this result validates our solar cell manufacturing.

The DSCs prepared with complex **C1** and electrolyte EL1 present V_{OC} = 550 mV, very close to the value obtained for N719, but a significant lower J_{SC} = 0.444 mA/cm^2. This leads to an overall conversion efficiency η = 0.324%, which is the best performance achieved with complex **C1**. The photochemical parameters worsen when **C1** works in combination with electrolyte EL2: V_{OC} = 396 mV, J_{SC} = 0.378 mA/cm^2, η = 0.233%. The improved performance attained with electrolyte EL1 is due to the presence of 4-tert-butylpyridine (TBP) affecting the semiconductor-electrolyte interface. It is known that this additive deprotonates the TiO_2 surface by adsorption, consequently shifting the conduction band of the semiconductor toward negative potentials [40]. The recombination of the photo-injected electrons and the redox mediator is then reduced. Consequently, the open-circuit potential and thus the overall efficiency of C1-EL1 improve [41]. With the ionic liquid as electrolyte, the solar cells C1-EL3 result in even lower photochemical parameters, being V_{OC} = 256 mV, J_{SC} = 0.275 mA/cm^2, and η = 0.101%. In this case, the high viscosity of the electrolyte limits the diffusion of the redox mediator and the dye regeneration is thus not as good as for the iodide/triiodide redox couple. This ultimately diminishes the solar cell performance [42], as it is observed in our experiments.

The solar cells sensitized with complex **C2** exhibited similar performance than complex **C1**. The characteristic parameters obtained with electrolyte EL1 became worse: V_{OC} = 510 mV, I_{SC} = 0.306 mA/cm^2, η = 0.206%. Interestingly, the performance enhances when using electrolyte EL2: V_{OC} = 492 mV, I_{SC} = 0.397 mA/cm^2, η = 0.324%. The presence of TBP in this case does not improve the efficiency since it reacts thorough the nitrogen with the allenylidene ligand, thus degrading the complex. After solar exposure, DSCs changed their characteristic red color to dark yellow, revealing the nature of this reaction. Despite this disadvantage, the cells C2-EL2 continued working with a concomitant efficiency loss. Finally, the performance with the ionic liquid electrolyte was poor, with an efficiency η = 0.028%. The reduction of dye regeneration, in combination with the reactivity of complex **C2** with the nucleophiles of the ionic liquid explain the bad operation of C3-EL3 cells. The reaction of the allenylidene-ruthenium complex with N-based nucleophiles has been reported elsewhere and support this explanation [30].

Fill factors were similar in all cases, as shown in Table 1. Regarding V_{OC} and I_{SC}, the best results were obtained for the iodide/triiodide redox couple. This reveals a dye regeneration limited by diffusion that should be related to the nature of ruthenium complex and the counterions. The highest efficiencies are attained for cells C1-EL1 and C2-EL2, emphasizing the importance of N-based additives such as TBP. It is important to note that complex **C2** reacts with TPB leading to lower photochemical parameters. Overall, the values of the conversion efficiency obtained with the ruthenium complexes are low, despite their good UV–vis absorption. The major drawback seems to be the nature of the ligands that define the HOMO-LUMO energy levels, and then the electron injection controlling the overall performance. More studies are in progress with the aim of further improving the sensitizing properties of PTA-based ruthenium complexes through a proper design of the ligands.

4. Conclusions

We synthesize two new ruthenium complexes bearing PTA ligands and test them as photosensitizers in fully operating dye-sensitized solar cells: $[RuCl_2(mPTA)_3(H_2O)](CF_3SO)_3$ (**C1**) and $[Ru(C=C=CPh_2)Cp(PTA)(PPh_3)](CF_3SO_3)$ (**C2**). The complexes exhibit excellent absorption over a wide range of the spectrum. Complex **C1** is characterized by absorption peaks at 326 and 448 nm, whereas complex **C2** displays a peak at 338 nm and a broad absorption band located at 520 nm, similarly to dye N719. The performance of DSCs is evaluated for three electrolytes and compared to the standard N719. The electrochemical behavior found was similar for both complexes with a strong dependence on the type of the electrolyte. The best performance, η = 0.324%, was achieved for the iodide/triiodide redox mediator. Particularly, complex **C2** reacted with the additive 4-tert-butylpyridine (present in EL2) reducing the photon-to-current conversion efficiency. The performance was low compared to that of the N719. Nevertheless, the complexes are able to sensitize DSCs and they possess thermal and chemical stability under irradiation.

Acknowledgements

Authors acknowledge the support of Projects CTQ2015-67384-R and CTQ2017-90050-R (MINECO/FEDER). Thanks are also given to Junta de Andalucia PAI-research group FQM-317 and COST Action CM1302 (WG1, WG2). BSM is grateful for the Talent Hub Program co-funded by the European Union's Seventh Framework Program, Marie Skłodowska-Curie actions (Grant Agreement n° 291780), and Junta de Andalucia. AFB thanks the support of the Cernep Research Center; University of Almeria.

Appendix A. Supplementary data

Supplementary material related to this article can be found, in the online version, at doi:https://doi.org/10.1016/j.colsurfa.2018.06.003.

References

[1] A. Hagfeldt, G. Boschloo, L. Sun, L. Kloo, H. Pettersson, Dye-sensitized solar cells, Chem. Rev. 110 (2010) 6595–6663, http://dx.doi.org/10.1021/cr900356p.
[2] M. Grätzel, Photoelectrochemical cells, Nature 414 (2001) 338–344, http://dx.doi.org/10.1038/35104607.
[3] F.-T. Kong, S.-Y. Dai, K.-J. Wang, Review of recent progress in dye-sensitized solar cells, Adv. Optoelectron. 2007 (2007) 1–13, http://dx.doi.org/10.1155/2007/75384.
[4] A. Polizzotti, J. Schual-berke, E. Falsgraf, M. Johal, Dr. Vasilis Fthenakis (Ed.), Investigating new materials and architectures for Grätzel cells Third Gener. Photovoltaics, 2012, pp. 111–140, , http://dx.doi.org/10.5772/28223 Chapter 5 ISBN: 978-953-51- 0304-2.
[5] K. Hara, H. Arakawa, Dye-sensitized solar cells, Handb. Photovolt. Sci. Eng. (2003), pp. 663–700, http://dx.doi.org/10.1002/0470014008.
[6] G. Richhariya, A. Kumar, P. Tekasakul, B. Gupta, Natural dyes for dye sensitized solar cell: a review, Renew. Sustain. Energy Rev. 69 (2017) 705–718, http://dx.doi.org/10.1016/j.rser.2016.11.198.

[7] B. O'Regan, M. Grätzel, A low-cost, high-efficiency solar cell based on dye-sensitized colloidal TiO2 films, Nature 353 (1991) 737–740, http://dx.doi.org/10.1038/353737a0.
[8] N. Sekar, V.Y. Gehlot, Metal complex dyes for dye-sensitized solar cells: recent developments, Resonance 15 (2010) 819–831, http://dx.doi.org/10.1007/s12045-010-0091-8.
[9] Y. Chiba, A. Islam, Y. Watanabe, R. Komiya, N. Koide, L. Han, Dye-sensitized solar cells with conversion efficiency of 11.1%, Jpn. J. Appl. Phys. 45 (2006) L638–L640, http://dx.doi.org/10.1143/JJAP.45.L638.
[10] S. Mathew, A. Yella, P. Gao, R. Humphry-Baker, B.F.E. Curchod, N. Ashari-Astani, I. Tavernelli, U. Rothlisberger, M.K. Nazeeruddin, M. Grätzel, Dye-sensitized solar cells with 13% efficiency achieved through the molecular engineering of porphyrin sensitizers, Nat. Chem. 6 (2014) 242–247, http://dx.doi.org/10.1038/nchem.1861.
[11] F. Bella, C. Gerbaldi, C. Barolo, M. Grätzel, Aqueous dye-sensitized solar cells, Chem. Soc. Rev. 44 (2015) 3431–3473, http://dx.doi.org/10.1039/C4CS00456F.
[12] V. Sugathan, E. John, K. Sudhakar, Recent improvements in dye sensitized solar cells: a review, Renew. Sustain. Energy Rev. 52 (2015) 54–64, http://dx.doi.org/10.1016/j.rser.2015.07.076.
[13] N.T.R.N. Kumara, A. Lim, C.M. Lim, M.I. Petra, P. Ekanayake, Recent progress and utilization of natural pigments in dye sensitized solar cells: a review, Renew. Sustain. Energy Rev. 78 (2017) 301–317, http://dx.doi.org/10.1016/j.rser.2017.04.075.
[14] A. Andualem, S. Demiss, Review on dye-sensitized solar cells (DSSCs), Rev. Dye Sol. Cells Edelweiss Appl. Sci. Technol. 2 (2018) 145–150, http://dx.doi.org/10.1016/j.rser.2016.09.097T4 Advanced techniques and research trends M4 - Citavi.
[15] A.S. Polo, M.K. Itokazu, N.Y. Murakami Iha, Metal complex sensitizers in dye-sensitized solar cells, Coord. Chem. Rev. 248 (2004) 1343–1361, http://dx.doi.org/10.1016/j.ccr.2004.04.013.
[16] L. Spiccia, G.B. Deacon, C.M. Kepert, Synthetic routes to homoleptic and heteroleptic ruthenium(II) complexes incorporating bidentate imine ligands, Coord. Chem. Rev. 248 (2004) 1329–1341, http://dx.doi.org/10.1016/j.ccr.2004.04.008.
[17] G.C. Vougioukalakis, A.I. Philippopoulos, T. Stergiopoulos, P. Falaras, Contributions to the development of ruthenium-based sensitizers for dye-sensitized solar cells, Coord. Chem. Rev. 255 (2011) 2602–2621, http://dx.doi.org/10.1016/j.ccr.2010.11.006.
[18] A. Reynal, E. Palomares, Ruthenium polypyridyl sensitisers in dye solar cells based on mesoporous TiO2, Eur. J. Inorg. Chem. (2011) 4509–4526, http://dx.doi.org/10.1002/ejic.201100516.
[19] Y. Qin, Q. Peng, Ruthenium sensitizers and their applications in dye-sensitized solar cells, Int. J. Photoenergy 2012 (2012), http://dx.doi.org/10.1155/2012/291579.
[20] P.G. Bomben, K.C.D. Robson, B.D. Koivisto, C.P. Berlinguette, Cyclometalated ruthenium chromophores for the dye-sensitized solar cell, Coord. Chem. Rev. 256 (2012) 1438–1450, http://dx.doi.org/10.1016/j.ccr.2012.02.005.
[21] M. Serrano Ruiz, A. Romerosa, B. Sierra-Martin, A. Fernandez-Barbero, A water soluble diruthenium-gold organometallic microgel, Angew. Chem. Int. Ed. 47 (2008) 8665–8669, http://dx.doi.org/10.1002/anie.200803232.
[22] E.M.J. Johansson, A. Sandell, H. Siegbahn, H. Rensmo, B. Mahrov, G. Boschloo, E. Figgemeier, A. Hagfeldt, S.K.M. Jönsson, M. Fahlman, Interfacial properties of photovoltaic TiO2/dye/PEDOT-PSS heterojunctions, Synth. Met. 149 (2005) 157–167, http://dx.doi.org/10.1016/j.synthmet.2004.12.004.
[23] F. Joó, J. Kovács, Á. Kathó, A.C. Bényei, T. Decuir, D.J. Darensbourg, A. Miedaner, D.L. Dubois, (Meta- sulfonatophenyl) diphenylphosphine, sodium salt and its complexes with rhodium(i), ruthenium(II), iridium(i), Inorg. Synth. (2007) 1–8, http://dx.doi.org/10.1002/9780470132630.ch1.
[24] P.S. Hallman, T.A. Stephenson, G. Wilkinson, Tetrakis(triphenylphosphine)dichlororuthenium(II) and Tris(triphenylphosphine)dichlororuthenium(II), Inorg. Synth. vol. XII, (1970), pp. 237–240, http://dx.doi.org/10.1002/9780470132432.ch40.
[25] B. Cornils, W.A. Hermans (Eds.), Aqueous-Phase Organometallic Catalysis, Wiley-VCH, Weinheim, Germany, 1998.
[26] D.N. Akbayeva, L. Gonsalvi, W. Oberhauser, M. Peruzzini, F. Vizza, P. Brüggeller, A. Romerosa, G. Sava, A. Bergamo, Synthesis, catalytic properties and biological activity of new water soluble ruthenium cyclopentadienyl PTA complexes [(C5R5)RuCl(PTA)2] (R = H, Me; PTA = 1,3,5-triaza-7-phosphaadamantane), Chem. Commun. (Camb) (2003) 264–265, http://dx.doi.org/10.1039/B210102E.
[27] A. Romerosa, T. Campos-Malpartida, C. Lidrissi, M. Saoud, M. Serrano-Ruiz, M. Peruzzini, J.A. Garrido-Cárdenas, F. García-Maroto, Synthesis, characterization, and DNA binding of new water-soluble cyclopentadienyl ruthenium(II) complexes incorporating phosphines, Inorg. Chem. 45 (2006) 1289–1298, http://dx.doi.org/10.1021/ic051053q.
[28] A. Romerosa, M. Saoud, T. Campos-Malpartida, C. Lidrissi, M. Serrano-Ruiz, M. Peruzzini, J.A. Garrido, F. García-Maroto, DNA interactions mediated by cyclopentadienidoruthenium(II) complexes containing water-soluble phosphanes, Eur. J. Inorg. Chem. (2007) 2803–2812, http://dx.doi.org/10.1002/ejic.200601177.
[29] R. Girotti, A. Romerosa, S. Mañas, M. Serrano-Ruiz, R. Perutz, Photo-aquation of cis-[RuCl2(mPTA)4](CF3SO3)4 in water (mPTA = N-methyl-1,3,5-triaza-7-phosphaadamantane), Dalton Trans. 40 (2011) 828–836, http://dx.doi.org/10.1039/c0dt00885k.
[30] M. Serrano-Ruiz, C. Lidrissi, S. Mañas, M. Peruzzini, A. Romerosa, Synthesis, reactivity and catalytic properties of the allenylidene [Ru(C=C=CPh2)Cp(PTA)(PPh3)](CF3SO3) (PTA = 1,3,5-triaza-7-phosphaadamantane), J. Organomet. Chem. 751 (2014) 654–661, http://dx.doi.org/10.1016/j.jorganchem.2013.08.040.
[31] A.A. Ramadan, R.D. Gould, A. Ashour, On the Van der Pauw method of resistivity measurements, Thin Solid Films 239 (1994) 272–275, http://dx.doi.org/10.1016/0040-6090(94)90863-X.
[32] C. Longo, M.A. De Paoli, Dye-sensitized solar cells: a successful combination of materials, J. Braz. Chem. Soc. (2003) 889–901, http://dx.doi.org/10.1590/S0103-50532003000600005.
[33] A.I. Maldonado-Valdivia, E.G. Galindo, M.J. Ariza, M.J. García-Salinas, Surfactant influence in the performance of titanium dioxide photoelectrodes for dye-sensitized solar cells, Sol. Energy 91 (2013) 263–272, http://dx.doi.org/10.1016/j.solener.2013.02.009.
[34] S. Ito, Facile fabrication of mesoporous TiO2 electrodes for dye solar cells: chemical modification and repetitive coating, Sol. Energy Mater. Sol. Cells 76 (2003) 3–13, http://dx.doi.org/10.1016/S0927-0248(02)00209-X.
[35] S. Ito, T.N. Murakami, P. Comte, P. Liska, C. Grätzel, M.K. Nazeeruddin, M. Grätzel, Fabrication of thin film dye sensitized solar cells with solar to electric power conversion efficiency over 10%, Thin Solid Films 516 (2008) 4613–4619, http://dx.doi.org/10.1016/j.tsf.2007.05.090.
[36] N. Hirata, J.J. Lagref, E.J. Palomares, J.R. Durrant, M.K. Nazeeruddin, M. Gratzel, D. Di Censo, Supramolecular control of charge-transfer dynamics on dye-sensitized nanocrystalline TiO2 films, Chem. A Eur. J. 10 (2004) 595–602, http://dx.doi.org/10.1002/chem.200305408.
[37] C.H. Tsai, S.Y. Hsu, C.Y. Lu, Y.T. Tsai, T.W. Huang, Y.F. Chen, Y.H. Jhang, C.C. Wu, Influences of textures in Pt counter electrode on characteristics of dye-sensitized solar cells, Org. Electron. Phys. Mater. Appl. 13 (2012) 199–205, http://dx.doi.org/10.1016/j.orgel.2011.10.020.
[38] A.F. Nogueira, C. Longo, M.A. De Paoli, Polymers in dye sensitized solar cells: overview and perspectives, Coord. Chem. Rev. 248 (2004) 1455–1468, http://dx.doi.org/10.1016/j.ccr.2004.05.018.
[39] Z.-S. Wang, H. Kawauchi, T. Kashima, H. Arakawa, Significant influence of TiO2 photoelectrode morphology on the energy conversion efficiency of N719 dye-sensitized solar cell, Coord. Chem. Rev. 248 (2004) 1381–1389, http://dx.doi.org/10.1016/j.ccr.2004.03.006.
[40] G. Boschloo, L. Häggman, A. Hagfeldt, Quantification of the effect of 4-tert-butylpyridine addition to I -/I3- redox electrolytes in dye-sensitized nanostructured TiO2 solar cells, J. Phys. Chem. B 110 (2006) 13144–13150, http://dx.doi.org/10.1021/jp0619641.
[41] S. Nakade, T. Kanzaki, W. Kubo, T. Kitamura, Y. Wada, S. Yanagida, Role of electrolytes on charge recombination in dye-sensitized TiO(2) solar cell (1): the case of solar cells using the I(-)/I(3)(-) redox couple, J. Phys. Chem. B 109 (2005) 3480–3487, http://dx.doi.org/10.1021/jp0460036.
[42] P. Cheng, W. Wang, T. Lan, R. Chen, J. Wang, J. Yu, H. Wu, H. Yang, C. Deng, S. Guo, Electrochemical characterization and photovoltaic performance of the binary ionic liquid electrolyte of 1-methyl-3-propylimidazolium iodide and 1-ethyl-3-methylimidazolium tetrafluoroborate for dye-sensitized solar cells, J. Photochem. Photobiol. A Chem. 212 (2010) 147–152, http://dx.doi.org/10.1016/j.jphotochem.2010.04.009.